Article:
Houghton, MR, Walkley, MA and Head, DA (2020) Anisotropic mechanical response of layered disordered fibrous materials. Physical Review E, 102 (6). 062502. ISSN: 2470-0045

https://doi.org/10.1103/PhysRevE.102.062502

Anisotropic Mechanical Response of Layered Disordered Fibrous Materials

M. R. Houghton, M. A. Walkley, and D. A. Head*
School of Computing, University of Leeds, Leeds LS2 9JT, United Kingdom
(Dated: November 18, 2020)

Mechanically bonded fabrics account for a significant portion of nonwoven products, and serve many niche areas of nonwoven manufacturing. Such fabrics are characterised by layers of disordered fibrous webs, but we lack an understanding of how such microstructures determine bulk material response. Here we numerically determine the linear shear response of needle-punched fabrics modeled as cross-linked sheets of 2D Mikado networks. We systematically vary the intra-sheet fiber density, inter-sheet separation distance, and direction of shear, and quantify the macroscopic shear modulus alongside the degree of affinity and energy partition. For shear parallel to the sheets, the response is dominated by intra-sheet fibers and follows known trends for 2D Mikado networks. By contrast, shears perpendicular to the sheets induce a softer response dominated by either intra-sheet or inter-sheet fibers depending on a quadratic relation between sheet separation and fiber density. These basic trends are reproduced and elucidated by a simple scaling argument that we provide. We discuss the implications of our findings in the context of real nonwoven fabrics.

I. INTRODUCTION

The nonwovens industry produces a broad range of different fabrics tailored for specific applications such as surgical face masks, fire fighting jackets, antibacterial wipes and artificial leather [1–3]. The suitability of each fabric for its intended application is dictated by a variety of design decisions at each stage of manufacturing, and many of these decisions are strongly influenced by the mechanical properties of the material. Designing new materials and modifying existing ones by experimental trial-and-error is a lengthy and costly process that depends on iteratively testing and re-manufacturing fabrics. Computational modelling can in principle accelerate the translation of new products from the lab to the commercial market by providing the capability to rapidly pre-screen putative formulations; however, any such tool would need to represent the fabric with sufficient fidelity to faithfully approximate real systems.

At the microscopic level, the webs of many nonwoven fabrics consist of randomly oriented and distributed networks of fibers. Similar networks from other domains have been successfully modeled using established flexible and semiflexible polymer theories [4–8]. The mechanical properties of individual polymers are well understood [9–11], but work in recent years has also allowed for a deeper understanding of collective fiber network mechanics [12–16]. In particular, work on Mikado networks has highlighted how the affinity of the response, i.e. the degree to which the microscopic deformation field follows the bulk strain, can be reduced for low fiber density and/or highly flexible fibers, resulting in a significant lowering of stiffness [17–21]. However, although anisotropy has been numerically investigated in two dimensions [22], layered networks in three dimensions have not been studied in this context.

In this manuscript we develop a model for layered fiber networks motivated by the nonwovens fabric industry, and use it to investigate the mechanical response as a function of controllable network parameters and the direction of the applied shear strain. In the generation of these networks, we take a simplified network representation similar to the permeability work of Mao and Russell [23], i.e. a series of networks that represent layered nonwoven fabrics that have been bonded through needlepunching, and provide a first understanding of the mechanics of needlepunched nonwovens through a systematic exploration of the macroscopic network anisotropy. Our primary findings are summarized in Fig. 1. We find that the response to a shear parallel to the sheet orientation is always dominated by the intra-sheet fibers that lie within the sheets, with the degree of affinity depending primarily on the network density. By contrast, perpendicular shear directions generate a much softer response that can be dominated by intra-sheet or the connecting inter-sheet fibres, depending on both fiber density and sheet separation in a manner that agrees with a simple scaling argument that we provide. It is hoped that the methodology and first insights generated by this work will lead to high-fidelity predictive tools for the nonwovens industry.

II. THE MODEL

Layered networks are generated by crosslinking a series of parallel two-dimensional random fiber sheets, and the linear mechanical response determined by minimizing the total network energy in response to a macroscopic strain applied at the boundaries. The geometry and mechanics of the networks are described separately below.

* d.head@leeds.ac.uk

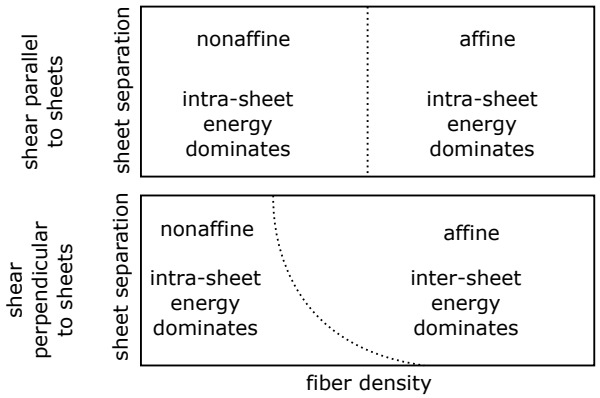

FIG. 1. A schematic summary of the dominant response regimes observed for our model. For a shear parallel to the sheets ('xy' in Fig. 2), the response is dominated by fibers lying within the sheets, with a degree of affinity that depends primarily on the fiber density. For perpendicular shears ('yz' and 'xz' in Fig. 2), the short fibers crosslinking the sheets dominate the response for high density and/or widely separated sheets, with a quadratic crossover that is derived in the main text.

A. Network Geometry

Unless otherwise stated, the simulation box is cubic with dimensions $W \times W \times W$, and contains a series of square $W \times W$ sheets aligned in parallel. Each sheet is a planar Mikado network of N elastic fibers of monodisperse length ℓ deposited with random orientations and positions, ensuring isotropy and mass homogeneity when each sheet is viewed on macroscopic length scales [17–20]. A total of M parallel sheets are placed in the simulation box with the same normal vector for each plane, flush to the cell walls, and with equal spacing h from adjacent sheets. Sheets are also contained within opposing fixed boundaries, thus there are $M = W/h + 1$ sheets in total, with $M - 2$ off-boundary sheets free to deform. For simplicity, rather than generate each sheet anew, the same Mikado network is repeated and rotated by $\pi/2$ between layers. This is sufficient to introduce disorder in the inter-sheet crosslinks as described below. That any systematic error arising from this rotation is at most small is evident from plots of the shear modulus against M in Appendix B, which shows no period 4 modulation for full rotations as would be expected if this choice was significant, but we cannot rule out more a significant contribution for *e.g.* networks placed under torsion, rather than the shears of interest here.

After generating the desired number of additional sheets, the network is cross-linked in two stages; intra-sheet followed by inter-sheet. Intra-sheet cross-linking is performed by identifying the points of intersection between filament pairs as per standard Mikado network generation. Each of these points is treated as a permanent and freely-rotating cross-link. Note that while there are a range of bonding techniques employed for non-woven fabrics, they are nonetheless often modelled as flexible bond points [2], thus the neglect of torques at cross-links is justified for this first investigation. It should also be noted that the choice between clamped and freely-rotating cross-links has been shown to make little difference far from the rigidity percolation transition [20], which is also the regime of interest here.

The mean distance between cross-links, as measured along a filament, is denoted ℓ_c, so the mean number of cross-links per filament is $\ell/\ell_c - 1$. Inter-sheet cross-links are then inserted between cross-link nodes lying in adjacent sheets, if the node separation is less than a tolerance $\ell_{\text{intra}} \geq h$, and with the constraint that each inter-sheet cross-link is mapped to at most one other cross-link from each of the neighbouring sheets. As constructed, inter-sheet crosslinks are short rod-like elements with nodes only at their ends, and thus can stretch but cannot bend. Further details are given in Appendix A.

To investigate the response under various imposed shears, the full network stack undergoes rigid body rotation prior to applying the same shear strain as shown in Fig. 2. We consider three sheet orientations labeled xy, yz and xz, referring to the planes in which the sheets lie, *i.e.* the third (absent) coordinate is constant for each sheet. The applied shear strain is always in the x–z plane as denoted in the figure. For simplicity and consistency across all considered network orientations, filaments are truncated at the box boundaries and all boundaries are fixed. Networks are deformed by a macroscopic shear strain γ by laterally translating the upper boundary $y = W$, with the lower boundary $y = 0$ kept fixed. All other boundaries affinely follow the same strain.

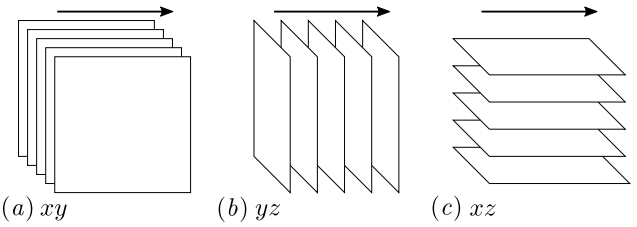

FIG. 2. Sheet networks sheared in 3 different orientations by prior rotation of the full geometry: xy (a), yz (b), and xz (c). Arrows show the applied shear direction for each orientation.

B. Network Energy

As in previous works [17–20], individual fibers are modeled as slender elastic bodies with deformation energies for both stretching/compression and bending. The energy cost for bending is based on the wormlike chain model [4], where non-zero curvature of the fiber midline incurs the energetic penalty

$$\mathcal{H}_{\text{bend}} = \frac{\kappa}{2} \int ds \left| \frac{\partial \hat{\mathbf{t}}}{\partial s} \right|^2 , \qquad (1)$$

for small curvatures, where the arc-length coordinate s is integrated along the total contour length of the filament, and $\hat{\mathbf{t}}$ is the tangent vector. Changes to the filament contour length incur a corresponding stretching energy cost

$$\mathcal{H}_{\text{stretch}} = \frac{\mu}{2}\int ds \left(\frac{d\ell(s)}{ds}\right)^2, \tag{2}$$

where $d\ell/ds$ represents the relative change in length along the filament, and μ is a stretching modulus. Both κ and μ can be given in terms of the cylindrical fiber's cross-sectional radius r and Young's modulus Y as $\kappa = (Y\pi r^4)/4$, $\mu = Y\pi r^2$. Thus the ratio of bending to stretching coefficients $\kappa/\mu = r^2/4$ is controlled by r, and Y sets the overall stress scale.

The Hamiltonian for the full network is constructed by linearly discretizing Eqs. (1) and (2) for all filament segments between cross-link nodes. As described above, intra-sheet filaments are free to stretch and bend, whereas the short connecting inter-sheet filaments may only deform through stretching (and compression). The desired shear is then applied at the boundaries, and the Hamiltonian is minimized to determine the microscopic network deformation that obeys static (athermal) mechanical equilbrium. All nodes other than those at the boundaries are allowed to move in an unrestricted manner, and since the rod configurations are fully specificied by the nodes, rod rotation is similarly unconstrained. In particular, intra-sheet rods are not constrained to rotate within the original plane of the sheets. The minimization is performed numerically, with the linear system solved using the sparse direct LU based MUMPS software package [24, 25] called externally through our model implementation in PETSc [26, 27]. These displacements are then used to calculate metrics of interest.

III. NUMERICAL RESULTS FOR ELASTIC MODULI

The area of each sheet is denoted A, so the line density of filaments within each sheet is $\rho = N\ell/A$ [20]. $M' = M - 2$ denotes the number of freely deforming sheets that contribute to the system energy, in addition to all inter-sheet crosslinking rods. Metrics calculated from the deformed network configurations include the total network energy, E, and the intra-sheet and inter-sheet energies, E_{in}, E_{out} respectively, defined as the network energy restricted to the corresponding subsets of filaments. The shear modulus G is related to E *via* $E/V = \frac{1}{2}G\gamma^2$ with $V = W^3$ the simulation box volume [28]. Unless otherwise stated the linear box dimension is $W = 2\ell$, the Young's modulus for the individual fibers is $Y = 1$, and the inter-sheet crosslink tolerance is $\ell_{\text{intra}} = 6h/5$.

A. Intra-sheet Filament Density

We first fix the number of sheets M and vary the overall filament density by controlling the number of intra-sheet filaments, *i.e.* the number per sheet N or equivalently the inter-sheet line density ρ. This in turn increases the number of inter-sheet cross-linking filaments. We denote the number of cross-linking filaments between sheets as N_{cf}. From Fig. 3(a), it is clear that the shear

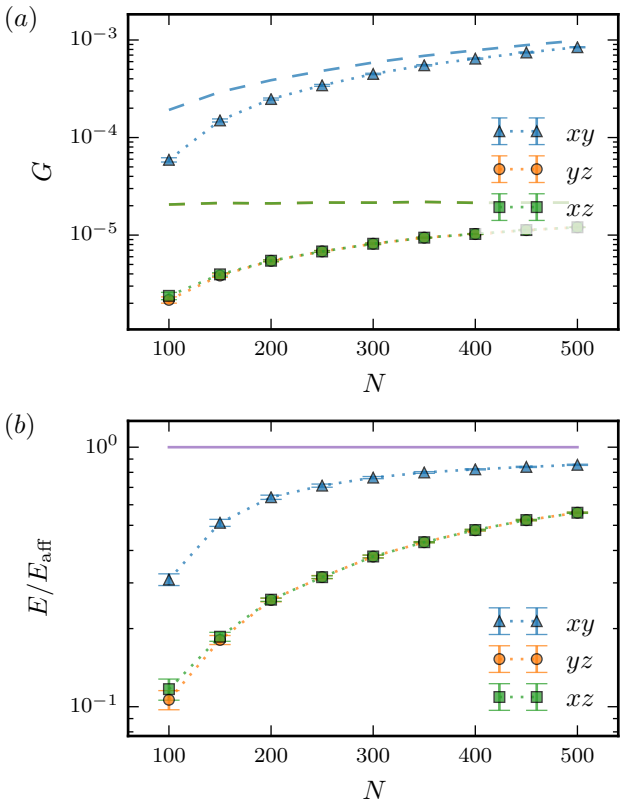

FIG. 3. (a) Shear modulus, G, and (b) energy, E, scaled to the affine prediction vs number of filaments per sheet, N, for three different shear directions. Sheet count and filament radius were fixed at $M = 5$ and $r = 1.996 \times 10^{-3}$ respectively. The dashed lines in (a) correspond to the affine predictions of the modulus, G_{aff}, for the respective shear directions.

modulus for all shear directions increases with increasing filament density, as expected. Moreover, shearing an xy oriented network produces a significantly larger shear modulus than the yz or xz oriented networks, for all of the tested filament densities. Network deformation also becomes more affine for higher density as demonstrated in Fig. 3(b), as in previous works [13, 17–20], with the xy orientation uniformly closer to affine that either the yz or xz orientations. The xy orientation shows a sharper initial increase towards affinity.

Fig. 4(a) shows that all orientations exhibit an increasing stretch energy contribution to the total energy as filament density is increased, and moreover the yz and xz orientations have a higher bending contribution to the to-

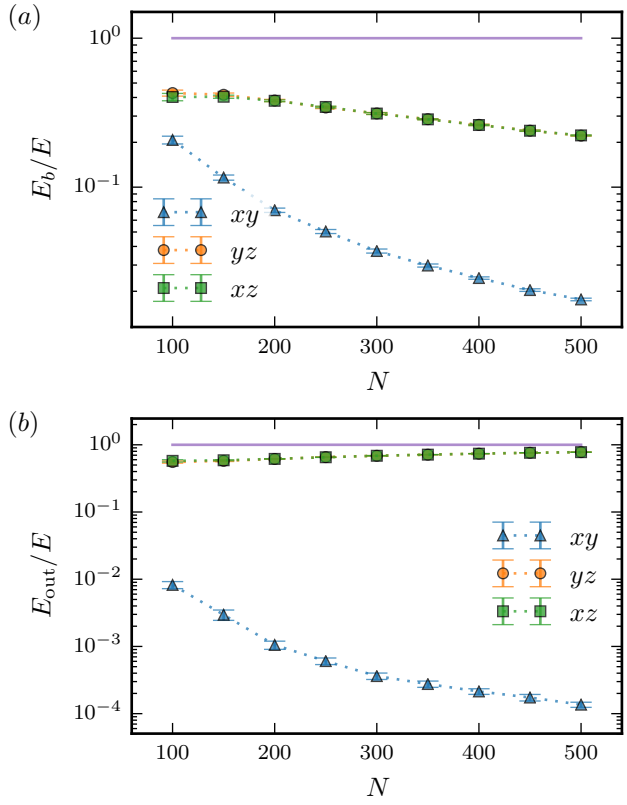

FIG. 4. Proportion of (a) bending energy to the total energy, E_b/E, and (b) inter-sheet energy to the total energy, E_{out}/E, vs number of filaments per sheet, N, for three different shear directions. Sheet count and filament radius were fixed at $M = 5$ and $r = 1.996 \times 10^{-3}$ respectively.

tal energy than xy orientations for the range of densities considered. The relative contribution of the inter-sheet energy E_{out} in shown in Fig. 4(b) and demonstrates opposing trends for different shear configurations – whereas the yz and xz orientations exhibit an increasing contribution due to E_{out} as the filament density increases, the contributions for xy orientations instead decreases. The relative contributions due to E_{out} are also uniformly lower for the xy orientation than either yz or xz. In all of plots discussed so far, there is a close correspondance in the yz and xz orientation data, with no significant difference between the two.

B. Sheet Separation Distance

To investigate the effect of sheet separation distance, recall that an increasing inter-sheet separation distance h corresponds to a decreasing sheet number M and *vice versa*, therefore h can be controlled by varying M in a fixed size box. Fig. 5 shows the shear modulus and energy per sheet varying M with a fixed number of filaments per sheet N. The shear modulus steadily decreases with increasing h for all of the shear orientations as shown in Fig. 5(a). However, this data is for fixed box size and

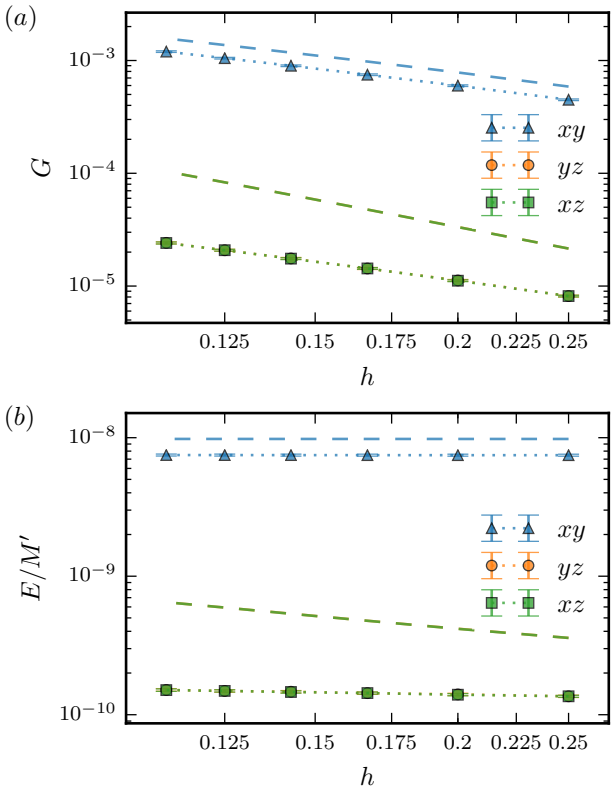

FIG. 5. (a) Total network shear modulus, G, and (b) energy per sheet, E/M', vs sheet separation distance, h, for three different shear directions, where $M' = M - 2$. Number of filaments per sheet and filament radius were fixed at $N = 300$ and $r = 1.996 \times 10^{-3}$ respectively. The dashed lines correspond to the affine predictions of the moduli for the respective shear directions.

thus a varying number of sheets. To get a clearer picture of the effect of increased sheet separation distance for fixed filament density, we can extract the energy corresponding to one sheet and a single set of connecting cross-linking filaments by scaling the total energy by the number of sheets; see Fig. 5(b) (note this definition neglects one layer of inter-sheet fibers). From this we observe a much weaker decrease in the energy per sheet for the yz and xz orientations, with no discernible variation for the xy orientation. There is a similar variation in the degree of affinity, with a weak but steady increase in affinity for the yz and xz orientations, but no visible variation for the xy orientation, as shown in Fig. 6.

Turning to the distribution of energies within the networks, Fig. 6 shows how affinity has no measurable dependence on separation distance for the xy oriented network, but increases with increasing separation distance for both the yz and xz orientations. Fig. 7(a) shows how increased sheet separation distance has no apparent effect on the ratio of bending to stretching energy for xy oriented networks, but promotes a higher contribution of stretching energy in the yz and xz oriented

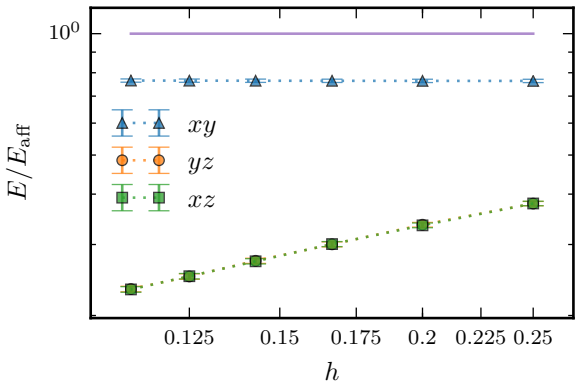

FIG. 6. Energy, E, scaled to the affine prediction vs sheet separation distance, h, for three different shear directions. Number of filaments per sheet and filament radius were fixed at $N = 300$ and $r = 1.996 \times 10^{-3}$ respectively.

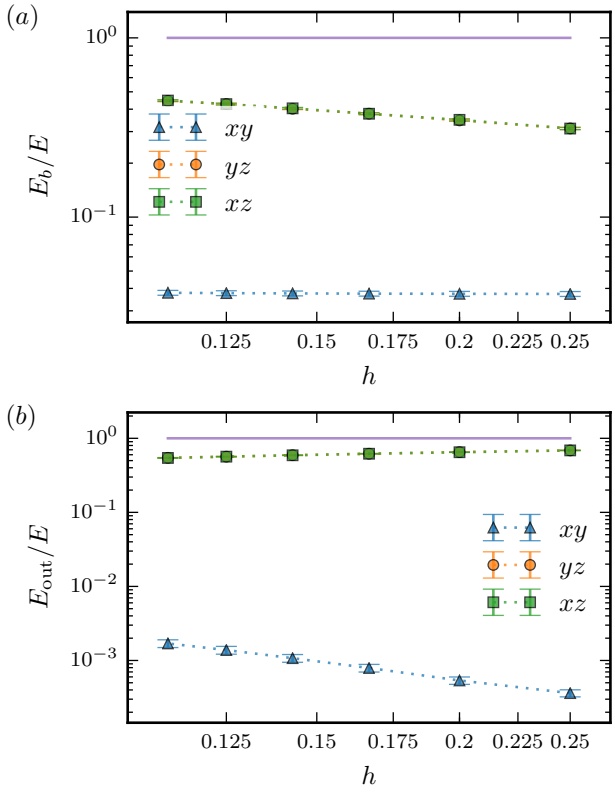

FIG. 7. Proportion of (a) bending energy to the total energy, E_b/E, and (b) inter-sheet energy to the total energy, E_{out}/E, vs sheet separation distance, h, for three different shear directions. Number of filaments per sheet and filament radius were fixed at $N = 300$ and $r = 1.996 \times 10^{-3}$ respectively.

networks. In terms of the intra-sheet/inter-sheet energy ratios, Fig. 7(b) demonstrates decreasing dependence of the total energy on inter-sheet energy for xy oriented networks as sheet separation increases, and increasing dependence on inter-sheet energy for yz and xz oriented networks.

C. Network Orientation

Thus far, no significant difference in the predicted mechanical properties of yz and xz oriented networks has been observed. To clarify the relationship between these network orientations, Fig. 8(a) shows the ratios of the shear modulus of the xy orientation, G_{xy}, yz orientation, G_{yz}, and xz orientation, G_{xz}, for increasing filament density, and Fig. 8(b) shows these same ratios for increasing

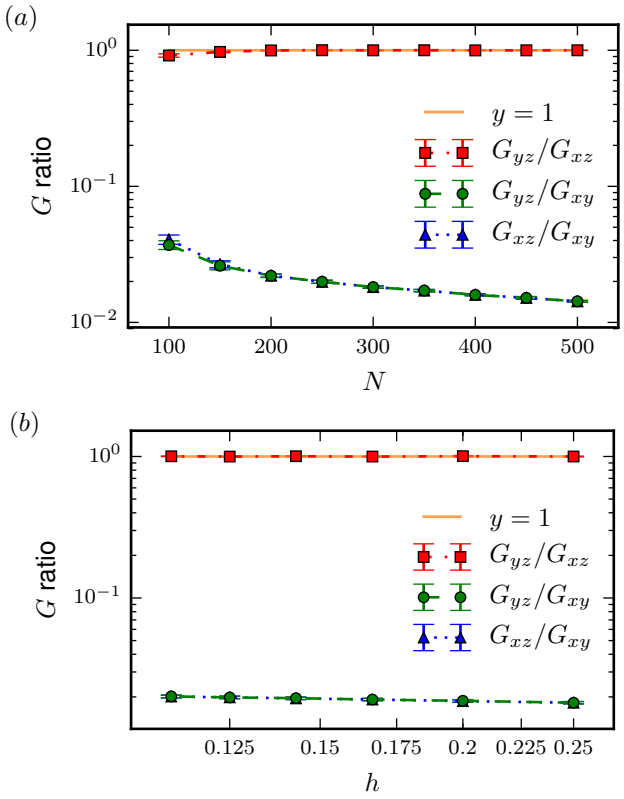

FIG. 8. Ratios of the shear moduli for each of the different shear directions plotted against (a) filament density per sheet, N, and (b) sheet separation distance, h.

sheet separation distance h. In no instance do the moduli for the yz and xz orientations exhibit any significant difference.

IV. DISCUSSION

We first derive approximate expressions for the various types of elastic energy under different shear orientations, before using these to aid in the interpretation of data systematically varying both the intra-sheet fiber density and the sheet separation.

A. Energy Scaling

Using arguments given in Appendix C, the expected number of cross-links within a single sheet is $\langle n_\times \rangle \propto \rho^2$, with a numerical prefactor that depends on the boundary conditions. Since $\rho = N\ell/A$, we can immediately infer that $\langle n_\times \rangle \sim N^2$. The number of connecting cross-linking filaments between sheets, N_{cf}, results from a 1-1 mapping between selected cross-links, thus $N_{cf} \sim \langle n_\times \rangle$ with some undetermined constant of proportionality. It follows that N_{cf} should also scale with N^2, as confirmed by Fig. 13, where a line can be fit to give an exponent of 2.0078 with an error of 6.7×10^{-3}. Assuming the range for inter-sheet cross-linking ℓ_{inter} is relatively only slightly larger than h, and the connected cross-links minimize the distance within the search tolerance (see Appendix A), the length of cross-linking filaments will be bounded below by, but close in value to, the separation distance, h, and generally oriented almost (but not exactly) perpendicular to the Mikado network sheets.

Our goal is to derive approximate expressions for the magnitudes of the different energy types in each shear orientation, to allow parameter ranges corresponding to dominant regimes to be predicted. We assume affine network deformation unless stated otherwise. The stretching energy of a single filament of length ℓ extending uniformly along its length with a total length change $\delta\ell$ is

$$E_s = \frac{1}{2}\frac{\mu}{\ell}\delta\ell^2, \tag{3}$$

as immediately inferred from (2). For intra-sheet filaments, we note that our assumption of affinity implies that extension is indeed uniform along the filament length, up to both end points, and uninterrupted by crosslinks. For the xy orientation under affine shear, intra-sheet filaments extend by a length $\delta\ell \sim \gamma\ell$, so that the energy of the filament scales as

$$\sim \frac{\mu}{\ell}(\gamma\ell)^2 \sim \mu\gamma^2\ell. \tag{4}$$

There is no intra-sheet filament extension for the yz or xz orientations under the assumption of the affinity. Note this is true for the yz orientation in linear response, as such sheets only extend to second order in the strain γ, *i.e.* in the non-linear response regime. This is a consequence of the symmetry, which requires the same sheet extension for $+\gamma$ as for $-\gamma$, so any extension must be even in γ, *i.e.* quadratic to leading order. To scale the single-filament stretching energy to the intra-sheet network, we multiply through by the number of intra-sheet filaments per unit area, N/A, to get

$$\frac{E_{\text{in}}^{\text{aff}}}{A} \sim \frac{N}{A}\mu\gamma^2\ell. \tag{5}$$

Using the definition of filament density $\rho = N\ell/A$, this is equivalent to

$$\frac{E_{\text{in}}^{\text{aff}}}{A} \sim \rho\mu\gamma^2. \tag{6}$$

For inter-sheet cross-linking filaments, we use the sheet separation distance, h, to approximate their length such that the spring constant is $k \approx \mu/h$. As confirmed by the explicit calculations provided in Appendix D, for all of the shear orientations considered, the extension under the assumption of affinity can be no more than $\sim \gamma h$, with a small prefactor as these filaments are almost perpendicular to the shear direction. Thus, the per-filament stretching energy is

$$\sim \frac{\mu}{h}(\gamma h)^2 \sim \mu\gamma^2 h. \tag{7}$$

As argued above and confirmed in Fig. 13, the number of cross-linking filaments per sheet per unit area scales with $\langle n_\times \rangle \sim \rho^2$, thus the total inter-sheet energy over all filaments per unit area scales with

$$\frac{E_{\text{out}}^{\text{aff}}}{A} \sim \frac{N_{cf}}{A}\mu\gamma^2 h \sim \rho^2\mu\gamma^2 h, \tag{8}$$

with a small numerical prefactor as noted above.

B. Discussion and Implications

Although the averaged deformation field matches the macroscopic affine prediction for any material, disordered media can achieve a lower energy response by deforming according to a non-affine displacement field, the precise form of which depends on the specific microstructural disorder. Nonetheless the affine scaling predictions $E_{\text{in}}^{\text{aff}}$ and $E_{\text{out}}^{\text{aff}}$ derived above can be used to guide understanding of trends in the results of the numerical experiments. We first discuss the xy shear orientation before turning to consider the yz and xz orientations together. As noted above and confirmed in Appendix D, the inter-sheet connecting rods can only stretch, and will do so only weakly as they lie almost perpendicular to the sheets for all of the shear orientations considered.

For the xy oriented networks, we observe that E_{in} is generally much larger than E_{out} over the parameter ranges considered, as demonstrated in Fig. 9(a). This is expected from the foregoing argument, as $E_{\text{out}}^{\text{aff}}$ has a very small numerical prefactor reflecting the near-perpendicularity of filaments to the shear. Consequently the total energy and total nonaffinity are largely independent of h, and follow similar trends to pure 2D sheets including increasing affinity and stretch-dominated response with increasing $\rho \sim N$; see Fig. 9(b) and Fig. 9(c). Nonaffine displacements reduce E_{in} and E_{out} below their respective affine predictions $E_{\text{in}}^{\text{aff}}$ and $E_{\text{out}}^{\text{aff}}$, in a manner that minimizes the total network energy $E = E_{\text{in}} + E_{\text{out}}$. There is no reason to expect the same set of nodal displacements to maximally reduce both E_{in} and E_{out}, thus intra-sheet and inter-sheet non-affinity will compete, with an increase in one coming at the expense of a decrease in the other. From Eqs. (6) and (8), we note that $E_{\text{out}} \sim \rho h E_{\text{in}}$. Thus for larger ρ and h, energy minimization will select for a greater reduction in E_{out} and a

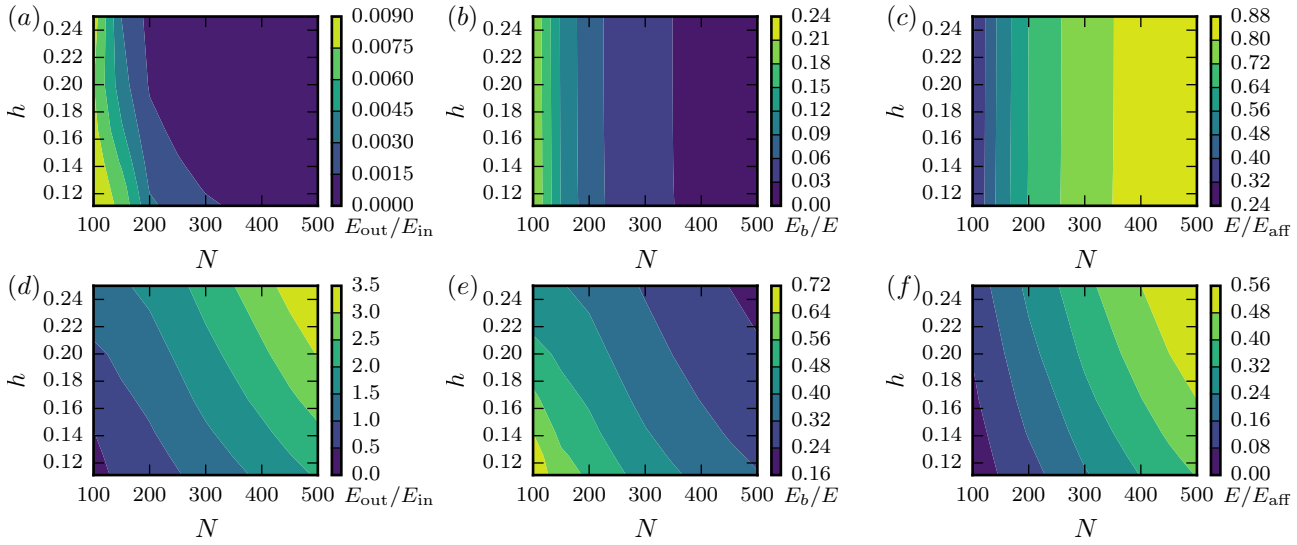

FIG. 9. Sheet separation distance, h, vs number of filaments per sheet, N, coloured by the ratio of inter-sheet to intra-sheet energy, $E_{\text{out}}/E_{\text{in}}$, in the (a) xy and (d) xz shear directions, the proportion of bending energy to total energy, E_b/E, in the (b) xy and (e) xz shear directions and the energy, E, scaled to the affine prediction in the (c) xy and (f) xz shear directions.

reduction in the ratio $E_{\text{out}}/E_{\text{in}}$, as confirmed in Fig. 9$(a)$. Conversely, node displacements that primarily reduce E_{in} are expected for small ρ and/or h. Thus although we still expect $E_{\text{out}}/E_{\text{in}} \ll 1$, it should be higher for low ρ, h, as confirmed by the figure.

For yz and xz orientations, the affine prediction for the intra-sheet energy is now zero, $E_{\text{in}}^{\text{aff}} = 0$, whereas the inter-sheet affine energy prediction scales as in Eq. (8) $E_{\text{out}}^{\text{aff}}/A \sim \rho^2\mu\gamma h$. Nonaffine deformations will again act to minimize the total energy, but in this case will now increase E_{in} from zero. For the range of network parameters considered here, E_{out} is not expected to be significantly reduced from $E_{\text{out}}^{\text{aff}}$ by nonaffine deformations, and we therefore expect $E_{\text{out}} \sim \rho h E_{\text{in}}$ to hold approximately true, as supported by Fig. 9(d). As with the xy oriented networks, the degree of affinity of the yz and xz oriented networks broadly increases with ρ and h as shown in Fig. 9(f). This suggests that the increase in affinity derives from increasing constraints imposed by the inter-sheet cross-links for increasing ρh, similar to the increased affinity with ρ in 2D Mikado networks [17–20].

V. SUMMARY

While many fiber network models consider isotropic and homogeneous Mikado networks of randomly oriented fibers, a range of industrial materials can be better modeled as layers of 2D Mikado sheets, with inter-sheet linking fibers providing mechanical integrity. In our investigation into this form of anisotropy, we generated predictions for the linear mechanical properties of such networks under imposed shear, and clarified the relationship between yz and xz shear directions. We have identified the dominant microscopic mechanisms that explain the measured bulk response by extracting the relevant quantities from our numerical solutions, confirmed by a simple scaling argument that, with further development, could be extended to also explain the observed trends in the ratio of fibre bending to stretching energy. Furthermore, we see that while the xy oriented networks follow similar trends to known results for 2D Mikado sheets, the competition between E_{in} and E_{out} allows E_{in} to be reduced below the affine prediction $E_{\text{in}}^{\text{aff}}$ in this xy case, and leads to a reduction in the total energy cost in the yz and xz oriented networks at the expense of an increase in E_{in} from 0.

It would be interesting to see if experiments on materials with comparable network geometries would exhibit similar mechanical properties and trends to those predicted by our numerical model. Both the inter-sheet separation h and fiber density $\rho \sim N$ in Figs. 1 and 9 should be controllable by suitable synthesis methods, and testing for different shear directions presents no fundamental challenge for characterisation. With validation and further model development, this first investigation into the competition between intra- and inter-sheet energy could be used to guide the design and manipulation of new or existing nonwoven fabrics that are bonded through a mechanical process such as needlepunching. Specifically, these results could have implications for deciding layer frequency, separation distance, punch depth, and needle count, since needleboard design determines fabric cross-link density [2, p. 404].

ACKNOWLEDGMENTS

M.R.H would like to acknowledge the EPSRC for funding this work through a Doctoral Training Grant.

Appendix A: Inter-sheet Cross-linking

Cross-linking between sheets was performed as in Fig. 10. For every internal node n_i^a of every filament in sheet a, and every internal node n_j^b of every filament in an adjacent sheet $b = a+1$, the closest n_j^b to n_i^a was identified. If the separation between the two nodes exceeded a tolerance ℓ_{inter}, then n_i^a was left disconnected to sheet b, and the next node of sheet a was considered. If the separation is less than ℓ_{inter}, and n_j^b has not already been connected to any other nodes in sheet a, then a short fiber is added connecting nodes n_i^a and n_j^b. We acknowledge

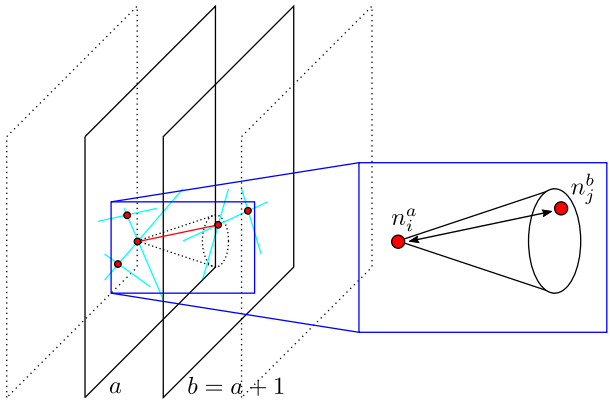

FIG. 10. An example of 1-1 cross-link mapping between sheets of a layered network. Each node n_i^a of sheet a has a conical search tolerance for finding the closest n_j^b of sheet b.

the possibility of introducing a small bias by assigning a direction to move between sheets (e.g. $b = a + 1$ rather than $b = a - 1$), but expect no significant difference to the mechanical properties for the networks and shears considered.

Appendix B: Finite Size Effects

Fig. 11 shows the effects of independently varying the area of the sheets at fixed line density ρ, and the number of sheets with fixed inter-sheet spacing h, on the measured shear modulus G in all 3 shear orientations. In both cases, any variation was much smaller than the error bars for the ranges considered, which corresponds to the parameter ranges investigated in the main text. We therefore conclude our basic findings are independent of system size effects. We further note there is no modulation of the shear stress with M, such as a period-4 effect that might be expected should our results be sensitive to the rotation of the sheets, as discussed in Sec. II A.

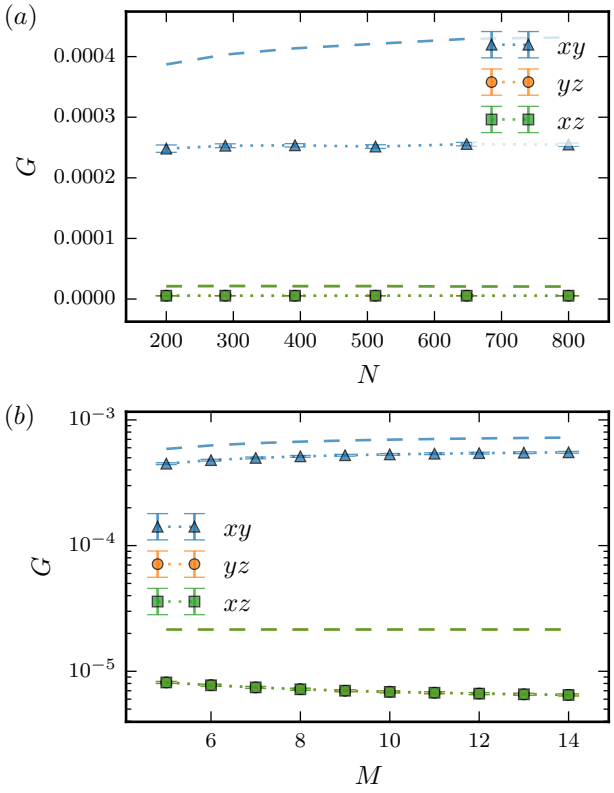

FIG. 11. Shear modulus, G, vs (a) sheet area quantified by the number of filaments N with the line density $\rho = 99.8$ fixed, and (b) the number of sheets with fixed sheet separation distance $h = 0.25$.

Appendix C: Cross-linking Density

To derive the cross-link density $\langle n_\times \rangle$ of a 2D network, we first consider $N = 2$ filaments of the same length ℓ, deposited onto a plane with random position and orientation. Denoting the relative angle between the filament pair θ, the region in which the midpoint of the second filament must fall to intersect the first filament, and hence form a single cross-link, is given by the parallelogram in Fig. 12). The area of this region is $A_\times = \ell^2 |\sin(\theta)|$, and averaging over θ gives

$$\langle A_\times \rangle = \frac{1}{\pi/2} \ell^2 \int_0^{\pi/2} d\theta \sin\theta = \frac{2\ell^2}{\pi}. \tag{C1}$$

Therefore, the probability of a randomly-deposited filament being cross-linked with one other filament in a plane of area A is

$$p_\times = \frac{A_\times}{A} = \frac{2\ell^2}{A\pi}. \tag{C2}$$

This assumes either an infinite plane, or one with dimenions $> \ell$ and periodic boundaries. For fixed boundaries

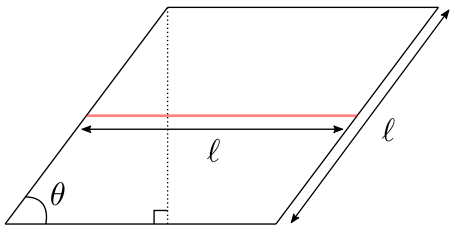

FIG. 12. Given the relative angle θ between a pair of filaments of length ℓ, the area in which a cross-link must lie is a parallelogram found by considering filament midpoints. For the red filament seen here, the midpoint of a second filament must lie somewhere in the parallelogram for the pair to intersect.

as employed in this manuscript, we expect the same scaling with ℓ and A, but a different numerical prefactor to $2/\pi$.

For $N > 2$, the expected number of cross-links per filament for large $N \gg 1$ is therefore

$$Np_\times = \frac{2N\ell^2}{A\pi} = \frac{2}{\pi}\rho\ell, \tag{C3}$$

in terms of the line density $\rho = N\ell/A$. Thus the total number of cross-links, avoiding double counting, is

$$\frac{N}{2}\left(\frac{2}{\pi}\rho\ell\right) = \frac{1}{\pi}N\rho\ell = \frac{N^2\ell^2}{\pi A}, \tag{C4}$$

and the total number of cross-links per unit area, $\langle n_\times \rangle$, is (C4) divided by A,

$$\langle n_\times \rangle = \frac{N^2\ell^2}{\pi A^2} = \frac{\rho^2}{\pi}. \tag{C5}$$

Without the numerical prefactor of $1/\pi$, this is the expression used in the main text.

Appendix D: Near-perpendicular fibers

Consider first the geometry in Fig. 14, in which an inter-sheet fibre is aligned almost perpendicular to the sheets in the xz orientation. In the coordinates indicated, the fibre has the end-to-end vector (Δ_x, Δ_y, h) and initial length $\ell_0 = \sqrt{\Delta_x^2 + \Delta_y^2 + h^2}$. Note that $\Delta_x = \Delta_y = 0$ corresponds to the exact perpendicular, and Δ_x and Δ_y can each be positive or negative.

Suppose an affine shear strain γ is applied as in the figure. Then the new end-to-end vector becomes $(\Delta_x + \gamma h, \Delta_y, h)$, with a new length $\ell_0 + \delta\ell = \sqrt{(\Delta_x + \gamma h)^2 + \Delta_y^2 + h^2}$. Expanding this in powers of γ,

$$\ell_0 + \delta\ell = \ell_0\left\{1 + \frac{\gamma h\Delta_x}{\ell_0^2} + \frac{(\gamma h)^2}{2\ell_0^4}\left(\ell_0^2 - \Delta_x^2\right) + \dots\right\},$$

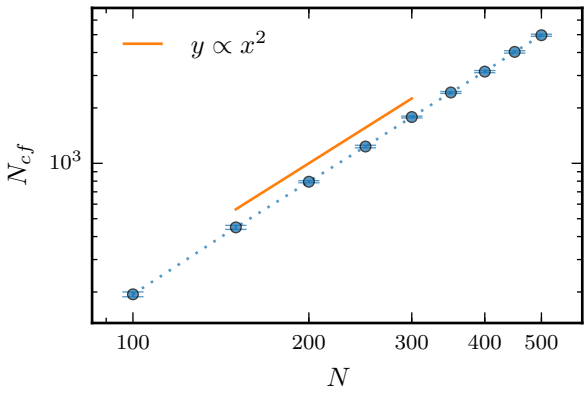

FIG. 13. The number of intra-sheet filaments per sheet per unit area, N, vs the inter-sheet cross-linking filaments per sheet per unit area, N_{cf}. The trend is quadratic as verified by the slope of $y \propto x^2$. Errors are no larger than the symbols here and throughout.

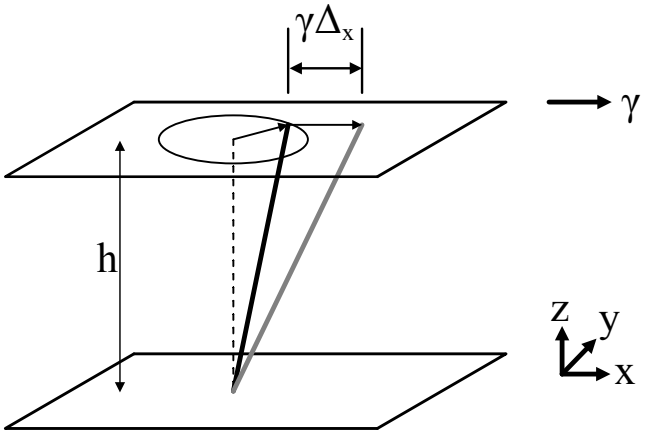

FIG. 14. Schematic of a single fibre (thick black line) with end-to-end vector (Δ_x, Δ_y, h), aligned nearly perpendicularly between two parallel sheets separated by a distance h. After a shear strain γ is applied, the fibre transforms to the vector $(\Delta_x + \gamma h, \Delta_y, h)$ (thick gray line).

so the linear extension for small strains $\gamma \ll 1$ is $\delta\ell \approx \frac{1}{\ell_0}\gamma h\Delta_x$, which vanishes for exactly perpendicular fibers with $\Delta_x = 0$. For almost perpendicular fibres with $\Delta_x, \Delta_y \ll h$, $\ell_0 \approx h$ and $\delta\ell \approx \gamma\Delta_x \ll \gamma h$, so the extension is small, even within the linear response regime. Since the stretching force is proportional to $\delta\ell$, the contribution to the stress tensor due to this fibre will be similarly small.

The discussion above was presented for sheets in the xz orientation, for which the end-to-end vector of the inter-sheet fibre is (Δ_x, Δ_y, h) as above. For xy sheet orientations, this vector can be written (Δ_x, h, Δ_z), which becomes $(\Delta_x + \gamma\Delta_z, h, \Delta_z)$ after shear. Repeating the calculations then gives the predicted linear extension $\delta\ell \approx \frac{1}{\ell_0}\gamma(\Delta_x)(\Delta_z)$. Finally, for the yz sheet orientation, the end-to-end vector changes from (h, Δ_y, Δ_z) to

$(h + \gamma\Delta_z, \Delta_y, \Delta_z)$, with an extension $\delta\ell \approx \frac{1}{\ell_0}\gamma h\Delta_z$. In all cases the same conclusions can be drawn, *i.e.* that the linear extension of near-perpendicular fibers is small, vanishing for exactly perpendicular fibers with all of the Δ's zero.

[1] I. M. Hutten, *Handbook of nonwoven filter media* (Elsevier, 2007).

[2] S. J. Russell, *Handbook of nonwovens* (Woodhead Publishing, 2006).

[3] A. F. Turbak, *Nonwovens: theory, process, performance, and testing* (TAPPI PRESS, 1993).

[4] M. Doi, S. F. Edwards, and S. F. Edwards, *The theory of polymer dynamics*, Vol. 73 (Oxford University Press, 1988).

[5] F. C. MacKintosh, J. Kas, and P. A. Janmey, Elasticity of Semiflexible Biopolymer Networks, Physical Review Letters **75**, 4425 (1995).

[6] T. Kim, W. Hwang, and R. D. Kamm, Computational Analysis of a Cross-linked Actin-like Network, Experimental Mechanics **49**, 91 (2009).

[7] M. L. Gardel, Elastic Behavior of Cross-Linked and Bundled Actin Networks, Science **304**, 1301 (2004).

[8] Y.-C. Lin, N. Y. Yao, C. P. Broedersz, H. Herrmann, F. C. MacKintosh, and D. A. Weitz, Origins of Elasticity in Intermediate Filament Networks, Physical Review Letters **104**, 058101 (2010).

[9] E. Farge and A. C. Maggs, Dynamic scattering from semiflexible polymers, Macromolecules **26**, 5041 (1993).

[10] F. Gittes, B. Mickey, J. Nettleton, and J. Howard, Flexural rigidity of microtubules and actin filaments measured from thermal fluctuations in shape., The Journal of cell biology **120**, 923 (1993).

[11] J. Wilhelm and E. Frey, Radial Distribution Function of Semiflexible Polymers, Physical Review Letters **77**, 2581 (1996).

[12] M. Tassieri, Dynamics of semiflexible polymer solutions in the tightly entangled concentration regime, Macromolecules **50**, 5611 (2017).

[13] P. R. Onck, T. Koeman, T. van Dillen, and E. van der Giessen, Alternative Explanation of Stiffening in Cross-Linked Semiflexible Networks, Physical Review Letters **95**, 178102 (2005).

[14] C. Heussinger and E. Frey, Role of architecture in the elastic response of semiflexible polymer and fiber networks, Physical Review E **75**, 011917 (2007).

[15] E. M. Huisman, C. Storm, and G. T. Barkema, Frequency-dependent stiffening of semiflexible networks: A dynamical nonaffine to affine transition, Physical Review E **82**, 061902 (2010).

[16] P. Muller and J. Kierfeld, Wrinkling of Random and Regular Semiflexible Polymer Networks, Physical Review Letters **112**, 094303 (2014).

[17] D. A. Head, A. J. Levine, and F. C. MacKintosh, Deformation of cross-linked semiflexible polymer networks, Physical review letters **91**, 108102 (2003).

[18] D. A. Head, A. J. Levine, and F. C. MacKintosh, Distinct regimes of elastic response and deformation modes of cross-linked cytoskeletal and semiflexible polymer networks, Physical Review E **68**, 061907 (2003).

[19] D. A. Head, F. C. MacKintosh, and A. J. Levine, Nonuniversality of elastic exponents in random bond-bending networks, Physical Review E **68**, 025101(R) (2003).

[20] J. Wilhelm and E. Frey, Elasticity of stiff polymer networks, Physical review letters **91**, 108103 (2003).

[21] M. Rubinstein, R. H. Colby, *et al.*, *Polymer physics*, Vol. 23 (Oxford University Press New York, 2003).

[22] A. R. Missel, M. Bai, W. S. Klug, and A. J. Levine, Affine-nonaffine transition in networks of nematically ordered semiflexible polymers, Physical Review E - Statistical, Nonlinear, and Soft Matter Physics **82**, 041907 (2010).

[23] N. Mao and S. Russell, Modeling permeability in homogeneous three-dimensional nonwoven fabrics, Textile research journal **73**, 939 (2003).

[24] P. R. Amestoy, I. S. Duff, J.-Y. L'Excellent, and J. Koster, A fully asynchronous multifrontal solver using distributed dynamic scheduling, SIAM Journal on Matrix Analysis and Applications **23**, 15 (2001).

[25] P. R. Amestoy, A. Guermouche, J.-Y. L'Excellent, and S. Pralet, Hybrid scheduling for the parallel solution of linear systems, Parallel Computing **32**, 136 (2006).

[26] S. Balay, S. Abhyankar, M. F. Adams, J. Brown, P. Brune, K. Buschelman, L. Dalcin, V. Eijkhout, W. D. Gropp, D. Karpeyev, D. Kaushik, M. G. Knepley, D. A. May, L. C. McInnes, R. T. Mills, T. Munson, K. Rupp, P. Sanan, B. F. Smith, S. Zampini, H. Zhang, and H. Zhang, *PETSc Users Manual*, Tech. Rep. ANL-95/11 - Revision 3.11 (Argonne National Laboratory, 2019).

[27] S. Balay, W. D. Gropp, L. C. McInnes, and B. F. Smith, Efficient management of parallelism in object oriented numerical software libraries, in *Modern Software Tools in Scientific Computing*, edited by E. Arge, A. M. Bruaset, and H. P. Langtangen (Birkhäuser Press, 1997) pp. 163–202.

[28] L. D. Landau, A. Kosevich, L. P. Pitaevskii, and E. M. Lifshitz, *Theory of elasticity* (Butterworth, 1986).